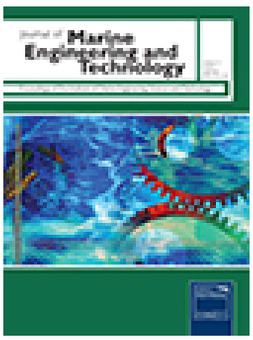

Journal of Marine Engineering & Technology

ISSN: 2046-4177 (Print) 2056-8487 (Online) Journal homepage: https://www.tandfonline.com/loi/tmar20

Design and parameter estimation of a remotely operated underwater vehicle

Yung-Lien Wang & Chang-Yu Lu

To cite this article: Yung-Lien Wang & Chang-Yu Lu (2012) Design and parameter estimation of a remotely operated underwater vehicle, Journal of Marine Engineering & Technology, 11:2, 39-48, DOI: 10.1080/20464177.2012.11020265

To link to this article: https://doi.org/10.1080/20464177.2012.11020265

Published online: 01 Dec 2014.

Design and parameter estimation of a remotely operated underwater vehicle

Yung-Lien Wang and Chang-Yu Lu, Department of Naval Architecture, National Kaohsiung Marine University, Nan-Tzu, Kaohsiung, Taiwan, ROC

The current study aims to design a remotely operated underwater vehicle (ROV) and estimate the parameters of a systematic model. The entire vehicle comprises the framework, propulsion instrument, sensor, and communication module. The systematic model is very complicated thus making it very difficult to obtain a transfer function of the entire system. Therefore, an experimental method is used to measure the acceleration of the vehicle when traversing underwater along a straight line. Moreover, the method is used to verify the transfer function of the vehicle's model for the entire system based on auto-regressive exogeneous (ARX) and auto-regressive moving average exogeneous (ARMAX) models, and a cost function.

AUTHORS' BIOGRAPHIES

Wang Yung-Lien received his BE and ME degrees in Mechanical Engineering from the National Taiwan Institute of Technology, Taiwan, ROC in 1991and 1993, respectively, and his PhD from the Department of Mechanical Engineering, National Cheng Kung University, Taiwan, in 1999. His research interests include compliant machines, mechatronics, precision engineering, image processing and robot fish.

Lu Chang-Yu received his BE degree from the Department of Naval Architecture and is a graduate student in the Institute of Ocean Engineering, National Kaohsiung Marine University, Taiwan.

INTRODUCTION

A remotely operated underwater vehicle (ROV) is mainly used in ocean ecology and topography, seabed search, inspection and maintenance of seabed cables, salvage, and port facilities. Complicated and changing underwater environments make the calculation and evaluation of the gravity centre, geometric centre of the shape, thrust, and other parameters of the vehicle extremely challenging. Thus the building of a vehicle model for the entire system is very difficult. Thus, the functional design of a vehicle and the construction of a systematic model will be the focus of this and future studies.

The need of the task is first determined in the design and manufacture of the vehicle. In previous studies, a roller-collector remotely operated vehicle (RC-ROV) was designed and used to search and collect objects.[1] The RC-ROV has a roller to collect objects, a camera to observe the seabed, and light emitting diode (LED) lighting. A modular design was adopted[2] to adjust and configure devices necessary for implementation of various tasks with an emphasis on the symmetry of the vehicle, direction of the propellers, and distance between devices. The vehicle was kept in the upright state using the righting moment generated by gravity and the buoyancy force.

A systematic model of a vehicle serves as a basis for the study of motion behaviour, controller and automatic navigation designs. Some researchers[3] built a system model by dynamic analysis, certain parameters of the model being directly measured on the vehicle and unknown parameters obtained using a 'gray-box' approach. Whereas previous studies[4] used a hydrodynamic propeller model and vehicle model to simulate vehicle motion, others[5,6] used least squares, extended least squares, recursive prediction error and model order to estimate the parameters. The current study describes straight-line navigation experiments from which data was obtained from a vehicle sensor. The data was subjected to frequency spectrum analysis and filtered appropriately to remove any noise components. On completion, a system

identification study was instigated using auto-regressive exogeneous (ARX) and auto-regressive moving average exogeneous (ARMAX) models with a cost function being utilised for comparison purposes. Thus from these models, system transfer functions of the vehicle were derived.

DESIGN ARCHITECTURE OF THE EXPERIMENTAL VEHICLE

The vehicle was designed using drawing software, and the architecture and dimension of the structural system were planned. The control system was configured based on the design scheme, and the mechanism part was designed using the module concepts, with emphasis on watertight design, experimental requirements, and counterweights. The control system was configured into four sub-parts, namely, power, communication module, drive, and sensor. An experiment was performed to verify the vehicle. Fig 1 shows the design procedure of the experimental vehicle.

In the modular design of the experimental vehicle structure, separate watertight modules were designed as it would be tested underwater and be frequently assembled, disassembled, and installed during the manufacture and testing, which may damage the watertight property. All the devices in the experimental vehicle adopted corresponding watertight methods, such as watertight bulkheads, to form independent watertight compartments for each device. Then an evaluation was made of the components capability and their watertight integrity methods. A 3D prototype based on the combination of the specific components and their dimensions was then developed and subjected to a simulation study. This procedure reduced unnecessary trials and provided accurate manufacturing data for future use.

Watertight design

A common watertight method is used by placing rubber at the seam where it is compressed and deformed to produce a restoring force that produces a watertight effect. An oil seal is used in the transmission shaft to prevent leakage of liquid from the revolving shaft and to deter dust and mud drifting in from the gap between the shaft hole and revolving shaft to the inside, which can affect the lifespan of the entire transmission mechanism.

The propulsion instrument, an important component of the vehicle, comprises an actuator and propeller. The actuator must be watertight because it operates in combination with the propeller through the revolving shaft. The revolving shaft passes through a convex flange disc, fixed onto a watertight box. A rubber washer is added between the flange disc and the watertight box, and they are compressed by the deformed rubber to prevent water from penetrating into the box via the fixing hole and to allow the actuator shaft to extend out of the box and combine with the propeller.

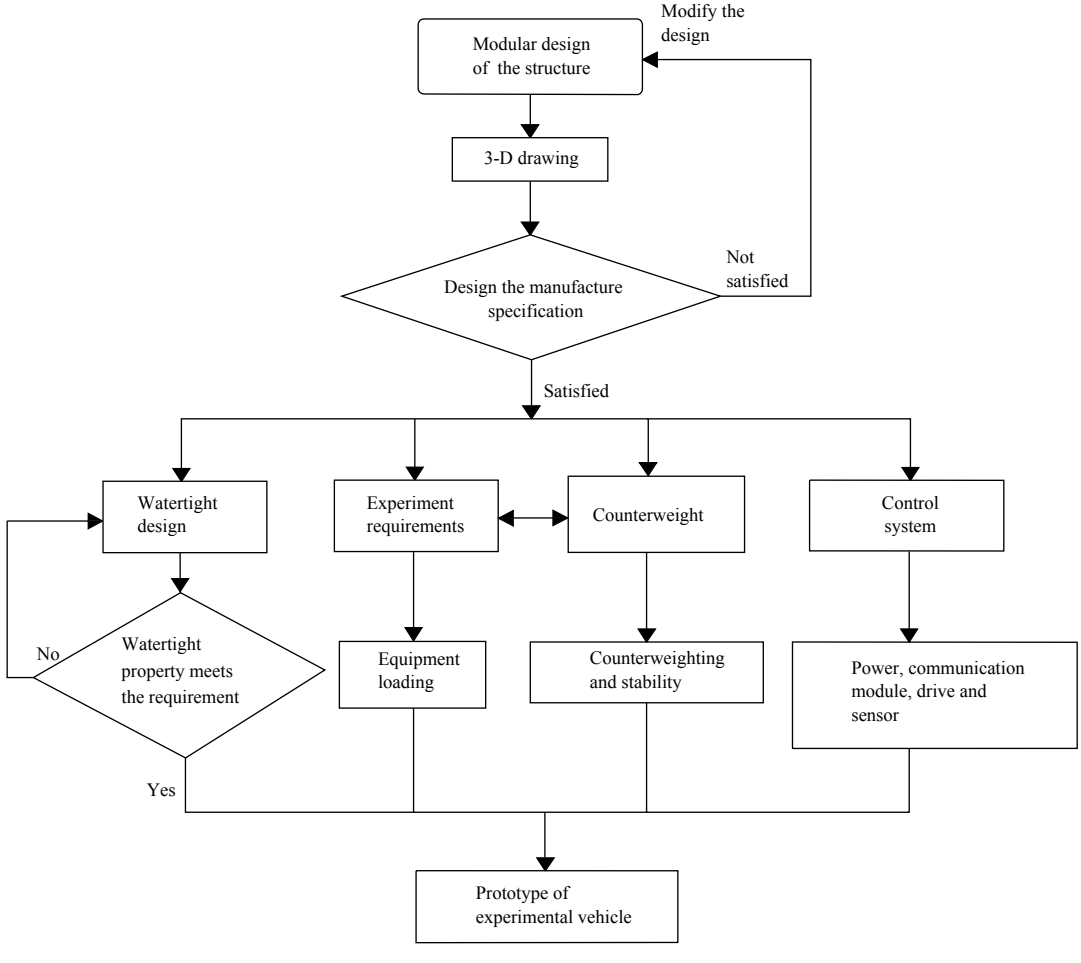

Fig 1: Experimental vehicle design procedure

Experimental requirements

As a tool for underwater study, the vehicle must fulfill various tasks, and devices are installed or removed according to experimental requirements. Thus, the devices on the vehicle adopt a modular design.

Counterweight

Various devices are installed on or removed from the experimental vehicle to change the gravity and geometric centres. The experimental vehicle does not have a uniform distribution of weight; hence, it cannot be directly used for experiments. Its stability must be adjusted in a water tank. The position of the counterweight must be tested and adjusted to attain the desired stability. A counterweight is then hung on the main structure of the experimental vehicle to reduce the complexity in adjusting the stability.

Control system

The vehicle is equipped with a main power supply [220V and 3300W (max)], a safety switch, and a 12V power supply for the communication module. All power supplies are put together and adopt an entirely watertight module. All other basic devices are divided into the communication module, drive, and sensor.

The control system can continuously receive data from the vehicle and outputs commands after storing, computing, and judgment, to control the vehicle's operation. Therefore, the control system builds files, calculates, and modifies the acceleration during operation of the experimental vehicle. The data can be used to verify the systematic model of the experimental vehicle. The sensor comprises an accelerometer and an angle gauge and adopts the printed circuit board layout for its circuit. The sensor detects the overall attitude of the experimental vehicle. Thus, it is installed at the centre of the main structure to reduce errors caused by shift when capturing sensor data.

The actuator and the propeller are important parts of the system. The test command signal is given by the communication module, and the thrust is produced on the propeller through the driven actuator to make the vehicle perform such actions as floating, diving, moving forward, and turning.

These devices are integrated and fastened to the experimental vehicle to complete the 3D design scheme, as shown in Fig 2. A fixation method is used to compress and fix the waterproof aluminum box to the aluminum arch.

COUNTERWEIGHT AND STABILITY OF THE EXPERIMENTAL VEHICLE

Watertight integrity and stability are important factors in the experimental vehicle, because any damage to the internal devices and will cause failure of the experiments and generate errors in the captured data. When the vehicle is counterweighted in the water tank, poor watertightness may cause leakage of water into the box, which can short and burn the devices inside it and change the gravity and geometric centres of the vehicle as a whole. Thus, the watertight property of the box needed to be determined before adjusting the stability.

The counterweight methods are divided into inside and outside counterweights, made of lead blocks or iron rods. The inside counterweight is placed inside a watertight box to balance and adjust stability. However, the vehicle cannot only be adjusted to the desired stability once during counterweighing, and the counterweight must be gradually changed to reach the desired stability. The vehicle must be lifted out of the water tank, and the watertight box must be opened to change the counterweight. However, the rubber washer on the watertight box will gradually experience fatigue and damage with an increasing number of changes, and the overall watertightness will be damaged, making the fixing of counterweights of different shapes difficult. Thus, a counterweight is hung outside so that the vehicle need not be lifted out of the water tank to change the counterweight, which reduces the complexity of counterweighing and avoids damage in the overall watertight performance of the counterweights. The outside counterweight therefore is used to adjust the stability of the vehicle.

For the purpose of stability adjustment, the vehicle can be regarded as a submerged body for analysis because it navigates underwater. Stability can be divided into static and dynamic components based on the motion condition of the vehicle. Dynamic stability means that the gravity and geometric centres of the vehicle as a whole continuously change when it navigates underwater, and thus, pitching and

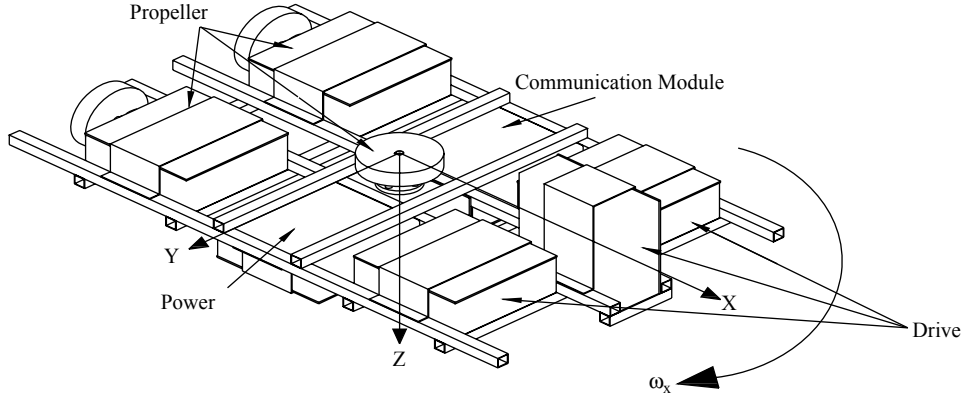

Fig 2: Structure of the experimental vehicle

rolling occur because of the influence of current fluctuation. Furthermore, the swinging angle of the vehicle constantly varies because of the inertia moment resulting from the varying rates of revolution of the propeller when the vehicle adjusts its forward motion and diving speed. Thus, dynamic stability must be adjusted using the change centre of gravity instrument. The fabrication process and the theoretical analysis are very complicated and will not be discussed in the current research. Therefore, only static stability is discussed herein.

Fig 3(a) shows that when the vehicle inclines because of the jolt caused by changing water flow or propeller speeds, the geometric centre (buoyancy centre) deviates by a distance of $<\overline{BG}>$. A righting moment initiated by gravity W and buoyancy force Δ restores the vehicle to its upright state. The theory behind this is that when counterweighing the vehicle in the water tank, a counterweight is hung below the vehicle and a buoyancy block is placed above to adjust the gravity G below the buoyancy centre B. For example, in horizontal stability, when the vehicle inclines, the gravity centre G is below the buoyancy centre B, resulting in a transverse righting moment $\Delta \times <\overline{BG}>$ sin α, where Δ is the buoyancy force that automatically restores the vehicle to the upright state and reaches stable equilibrium when it navigates underwater to prevent it from overturning and capturing wrong data. During adjustment of the vehicle, the lower the gravity centre is the longer is the distance between the gravity and buoyancy $<\overline{BG}>$ centres. In addition, the greater the arm of the righting force is, the greater is the righting moment resulting from the gravity and buoyancy force. Thus, when the vehicle navigates underwater and inclines because of current fluctuation and changes in the speed of the actuator, it can be rapidly restored to the upright state, as shown in Fig 3(b). When the vehicle inclines longitudinally, gravity and buoyancy forces at the geometric centre produce a righting moment $\Delta \times <\overline{BG}>$ sin β along the transverse inclination and restore the vehicle to the upright state based on the same theory of transverse stability.

After fabrication of the vehicle, it was counterweighted in the water to adjust the overall stability and prevent overturning during the experiments. A simple diving test was conducted after the vehicle was counterweighted to the upright state, as shown in Fig 4. The propeller at the Z-axis rotated to provide the diving force F. The vehicle was found to be subjected to additional buoyancy Δ_1 in the longitudinal stability during

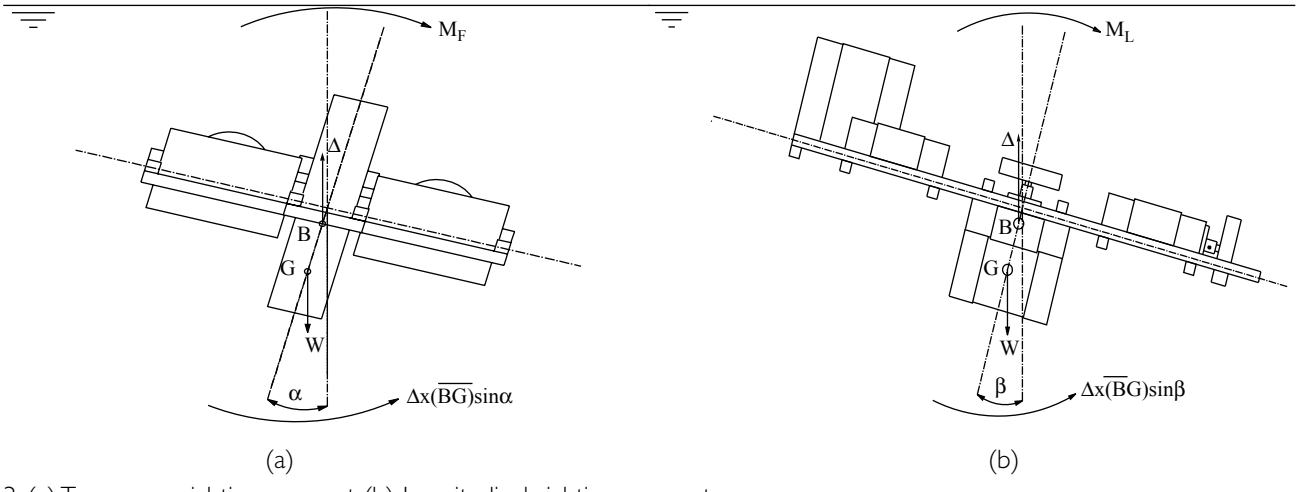

Fig 3: (a) Transverse righting moment (b) Longitudinal righting moment

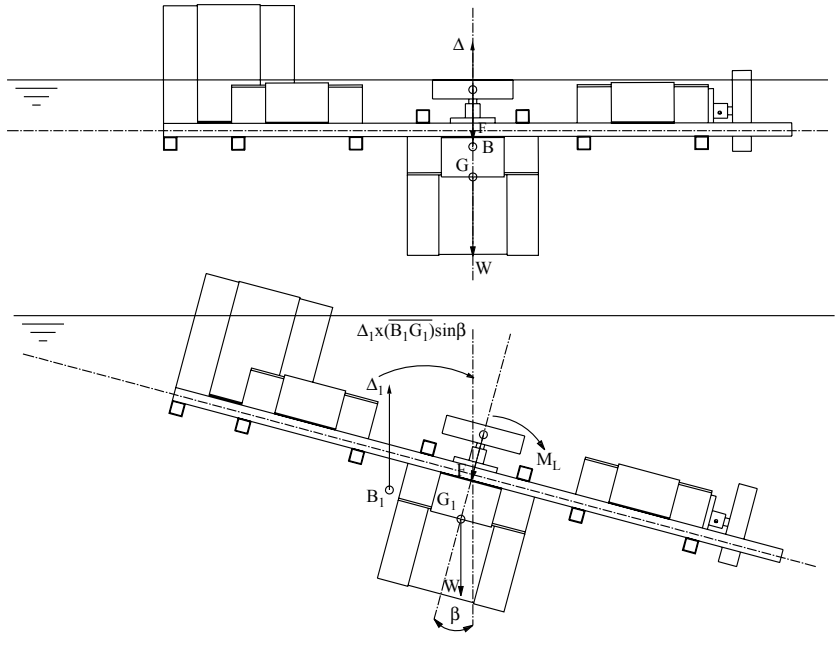

Fig 4: Drift of the buoyancy center when diving

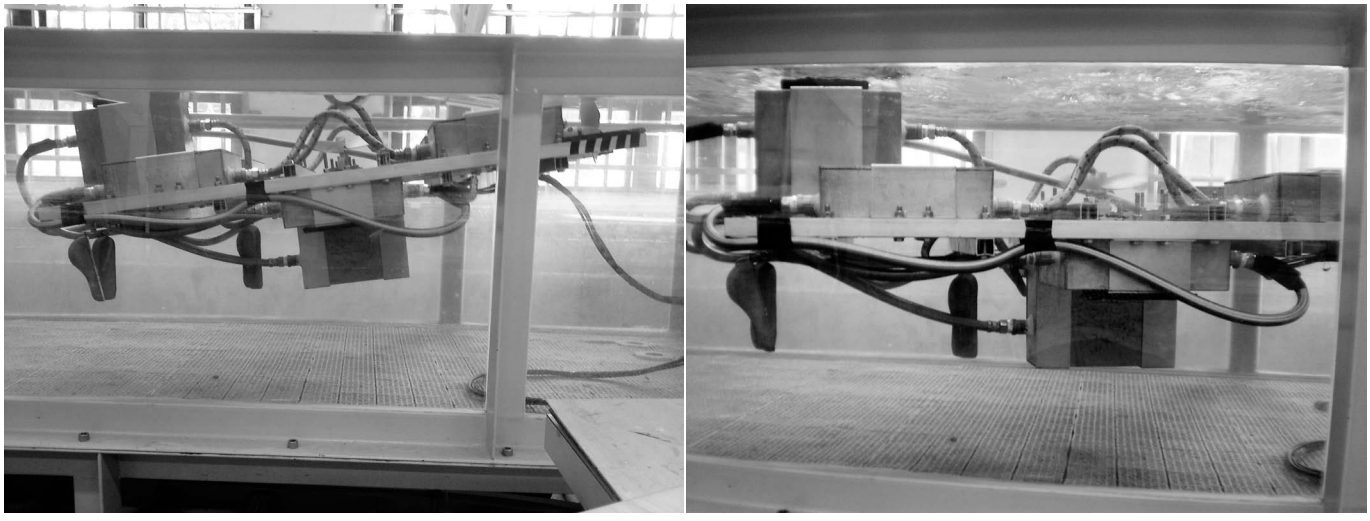

(a) (b)

Fig 5: Adjustment of the static stability and experimental testing

diving. Moreover, the position of the buoyancy centre B_1 and gravity centre G_1 changed after the middle drive sank into the water resulting in the new positions of B_1 and G_1 that are not in the same line and hence produced an overturning moment $\Delta \times <\overline{B_1G_1}> \cos \beta$. In addition, the propeller on the Z-axis cannot be precisely installed on the vehicle during assembly, and a moment M_L was produced at the centre of the entire vehicle, causing it to overturn during diving. Thus, another counterweight was required. An outside lead block counterweight was hung outside the main structure to hold the vehicle to the upright state during the diving test. The buoyancies at the front and back of the vehicle were found to differ significantly after the addition of the counterweight, similar to the previous situation without it. Thus, the buoyancy at the tail of the vehicle had to be increased to bring it to an oblique and stable balance state. The vehicle was then gradually restored to the upright state when diving, as shown in Fig 5.

INSTALLATION OF THE CONTROL SYSTEM

The control system in the vehicle is composed of power, communication, drive, and sensor modules. The control system functions in the following way: the computer accepts the speed command through the human–machine interface. The RS-232 signals output by the computer are converted to RS-485 signals for remote transmission to the vehicle via the communication module. The signals are converted to analogue voltage through the D/A module and input into the drive. The drive causes the actuator, together with the propeller, to produce the propelling force.

The acceleration data obtained from the vehicle are converted to RS-485 signals via the A/D module and transmitted to the communication module for conversion. The converted signals are then transmitted to and stored in the computer. Fig 6 shows the signal flow chart of the vehicle. In general, the control system can use analogue signals, digital signals and pulse width modulation (PWM) to control the actuator. In this study, uniform analogue signals for the control were used, which were convenient for the transmission and reception of data among the devices.

The communication module mainly uses I-7000 series remote I/O modules produced by ICP DAS. This series of modules includes analogue input and output, digital input and output, timer, frequency counter, RS-232 to RS-485 converter, and other functions. Based on the modular design of the vehicle, the communication module adopts the D/A conversion module (I-7024), A/D conversion module (I-7017R), and RS-232 to RS-485 signal conversion module (I-7561) in this series. In the module setting, I-7561 was first linked to the computer. Then, the I-7561, a virtual COM port built after the USB connection with the computer, is driven by a suitable software program.

The vehicle diving and forward motion is instigated through the propulsion unit and its overall speed is controlled by the drive and actuator in the control system (ASDA-AB

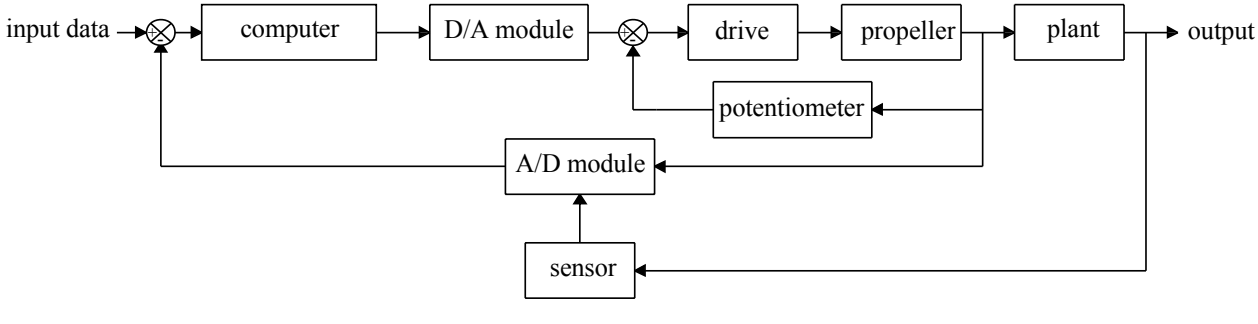

Fig 6: Signal flow chart of ROV

series produced by Delta Electronics. Drive model: ASD-A0421-AB, power: 400W, and working voltage: 220V). The transmission of the drive can be set up by the analogue and digital signals. The overall control system uses analogue signals.

The AC servo motor (actuator) is based on the different modes inside the drive used to provide different forms of actuation. The basic forms of a drive include position, speed, and torque. The current study mainly controls the speed of the actuator using the speed mode to control the speed of the vehicle underwater. The drive adjusts the speed of the actuator using the analogue voltage difference between *V*-REF and GND. The input voltage is between ±10V.

In this study, the sensor comprises an accelerometer (MMA7260Q), an angle gauge (ADXRS300), and other sensing components. The accelerometer and angle gauge detect the changes in acceleration and angle speed for forward motion and diving of the vehicle underwater. The sensor continuously captures the data as the vehicle navigates and transmits the data to an onshore signal conversion module. Finally, the data are stored in the computer from RS-485 to RS-232 signals. The stored data are important parameters for building a systematic model for the vehicle.

Fig 2 shows the sensing components of the sensor and the types of data captured during the experiment. The accelerometer captures acceleration on the *X* and *Z* axes (ie, changes in acceleration when moving forward and diving). The forward propulsion of the vehicle is produced by a double propeller. This propeller was not installed to the correct position during assembly due to manufacturing errors, resulting in inequality in the left and right thrusts and in the angular velocity along the *Z* axis when the vehicle advances. The angle gauge captures the change in angular speed when the vehicle navigates. Finally, the sensor transmits the speed to the onshore computer, which stores the files built through the communication module for future use in the system identification of the vehicle.

EXPERIMENTAL TESTING AND SYSTEM IDENTIFICATION

Testing and data capture process

During the navigation test, the vehicle advances at a fixed rotation speed, where each rotation speed is tested five times, and the results averaged to reduce the errors in the experimental process. The data were then used for system identification.

ARX and ARMAX models

The theoretical transfer function for the systematic model of the vehicle when navigating underwater is very complicated, and accuracy is greatly reduced. Thus, a general system identification method is adopted. A previous study[7] used ARX and ARMAX models to obtain transfer functions for single input, multi-output systems. Therefore, these two models have been extensively applied in various fields. They are directly applied to the vehicle to obtain the overall system parameters for future controller development studies.[8,9,10,11]

The ARX model is described by an invariant discrete system with single variables. *u(t)* and *y(t)* are the input and output signals for system sampling, respectively. A general *n*th-order differential equation is used to describe the input and output of ARX model of the vehicle as:

$$\begin{aligned} &y(t)+a_1y(t-1)+a_2y(t-2)+\cdots+a_{\mathrm{n}}y(t-\mathrm{n})\\ &=b_0\mathrm{u}(\mathrm{t})+b_1\mathbf{u}(\mathrm{t}-1)+\cdots+b_{\mathrm{n}}\mathrm{u}(\mathrm{t}-\mathrm{n})+e(\mathrm{t}) \end{aligned} \tag{1}$$

where $e(t)$ is the fitting error.

In Equation (1), the error term, $e(t)$, describes the sum of all disturbing factors and is replaced by a constant term. Thus, the simulation with parameters estimated through system identification has a bigger error compared with the experimental result. $e(t)$ is modified to the moving average of the fitting error to reduce the error.

A model can be obtained as:

$$\begin{aligned} &y(t)+a_1y(t-1)+a_2y(t-2)+\cdots+a_{\mathrm{n}}y(t-\mathrm{n})=\\ &b_0\mathrm{u}(\mathrm{t})+b_1\mathbf{u}(\mathrm{t}-1)+\cdots+b_{\mathrm{n}}\mathrm{u}(\mathrm{t}-\mathrm{n})+e(\mathrm{t})+\\ &c_1e(t-1)+\cdots+c_ne(t-n) \end{aligned} \tag{2}$$

As the moving average term of the fitting error is added, Equation (2) is known as the ARMAX model and is a standard tool for estimating parameters. The current study uses the ARX and ARMAX models as methods for estimating the system parameters of the vehicle.

System identification of vehicle

The operative procedure of system identification was conducted in the open loop using a step input signal and the acceleration response data was collected. A model is built for the entire system of the vehicle using the ARX and ARMAX models. Moreover, the systematic model of the vehicle is decided with the minimum value of the cost function. The cost function is built using the error between the experimental and simulation results of the model. Thus, the cost function can be defined as:

$$J=\frac{1}{n}\left(\sum_{i=1}^{n}(y(t_i)-\hat{y}(t_i))^2\right) \tag{3}$$

where $y(t_i)$ and $\hat{y}(t_i)$ are the experimental and simulation results of the model, respectively.

As the experimental environment has many interfering elements, the experimental data must be filtered before the parameter estimation. First, the data are analysed using FFT (Fast Fourier Transform) frequency analysis to find out the main frequency for 150 and 180 rpm (revolutions per minute).

Fig 7 shows the FFT spectrum of each rotation speed, where the main frequencies of 0.3 and 0.37Hz are twice the main frequencies of 0.6 and 0.74Hz as the filter frequencies for 150 and 180 rpm, respectively. The 0Hz in the figure corresponds to the testing signal of the step output, produced when the actuator starts. Thus, it is not taken as the frequency of the systematic model.

The ARX and ARMAX models built before and after filtration were compared. Finally, the optimum systematic model of the experimental vehicle was chosen based on the value of the cost function shown in Tables 1–4 (the *J* values

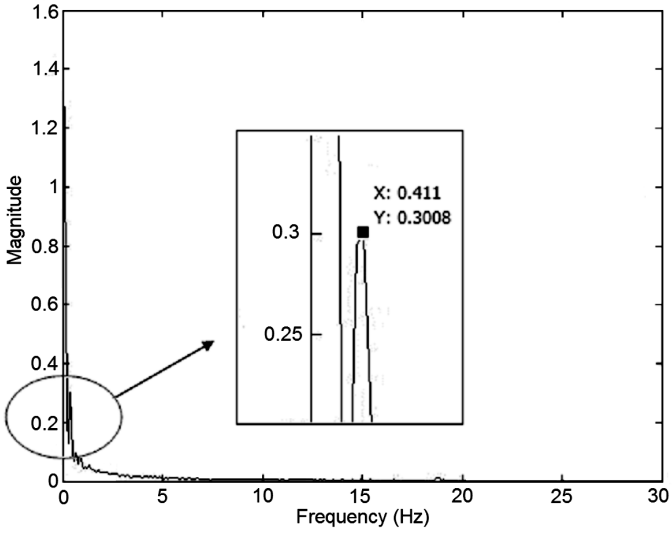

Fig 7(a): 150 rpm of FFT spectrum

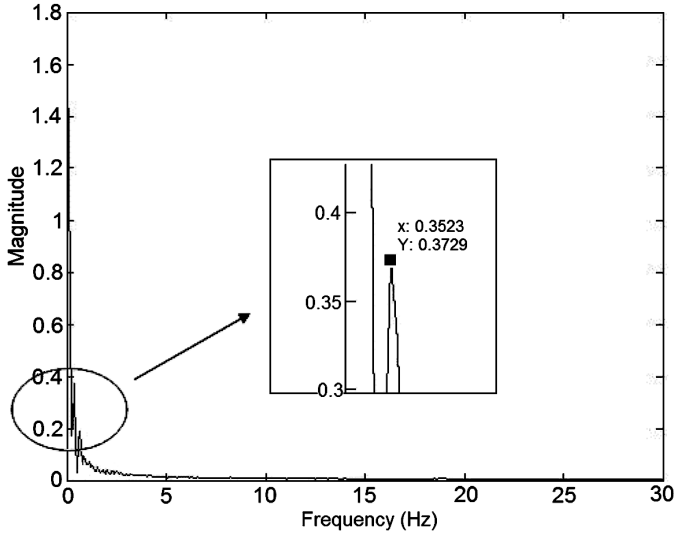

Fig 7(b): 180 rpm FFT spectrum

ARX Model	J before filtration	J after filtration
$a_n = 2, b_n = 0$	**0.0115601**	0.0042399
$a_n = 2, b_n = 1$	0.0124194	0.0028589
$a_n = 2, b_n = 2$	0.0121048	0.0021523
$a_n = 3, b_n = 0$	0.0122674	0.0037374
$a_n = 3, b_n = 1$	0.0128647	0.0022826
$a_n = 3, b_n = 2$	0.0124155	**0.0018944**
$a_n = 3, b_n = 3$	0.0135007	0.0041286

Table 1: ARX model and *J* values for 150 rpm

ARMAX Model	J before filtration	J after filtration
$a_n = 2, b_n = 0, c_n = 2$	0.0101951	0.0041604
$a_n = 2, b_n = 1, c_n = 2$	0.0097907	0.0050942
$a_n = 2, b_n = 2, c_n = 2$	0.0106906	0.0019699
$a_n = 3, b_n = 0, c_n = 3$	0.0125741	0.0046461
$a_n = 3, b_n = 1, c_n = 3$	0.0139927	0.0031883
$a_n = 3, b_n = 2, c_n = 3$	**0.0022807**	0.0017393
$a_n = 3, b_n = 3, c_n = 3$	0.0131479	**0.0017105**

Table 2: ARMAX model and *J* values for 150 rpm

ARX Model	J before filtration	J after filtration
$a_n = 2, b_n = 0$	**0.0090853**	0.0092849
$a_n = 2, b_n = 1$	0.0101508	0.0154368
$a_n = 2, b_n = 2$	0.0102757	0.0018249
$a_n = 3, b_n = 0$	0.0098463	0.0086059
$a_n = 3, b_n = 1$	0.0105076	0.0193399
$a_n = 3, b_n = 2$	0.0103592	**0.0018097**
$a_n = 3, b_n = 3$	0.0108514	0.0035649

Table 3: ARX model and *J* values for 180 rpm

ARMAX Model	J before filtration	J after filtration
$a_n = 2, b_n = 0, c_n = 2$	0.009163	0.0091354
$a_n = 2, b_n = 1, c_n = 2$	0.0091739	0.0133302
$a_n = 2, b_n = 2, c_n = 2$	**0.0031743**	0.0018029
$a_n = 3, b_n = 0, c_n = 3$	0.0098113	0.0126691
$a_n = 3, b_n = 1, c_n = 3$	0.0093401	0.0151292
$a_n = 3, b_n = 2, c_n = 3$	0.0084949	**0.0016982**
$a_n = 3, b_n = 3, c_n = 3$	0.0111072	0.0057081

Table 4: ARMAX model and *J* values for 180 rpm

of the cost function of the actual and simulation data for 150 rpm and 180 rpm, respectively). Figs 8(a–d) show the best fitting curves of each revolution speed of the ARX and ARMAX models.

ANALYSIS OF THE SYSTEMATIC MODEL

Based on the *J* values of the cost function in the previous section, the simulation result obtained from the moving average after the addition of $e(t)$ into the ARMAX model was closer to the experimental data than that in the ARX model. Thus, the experimental data are filtered to reduce the interference of noise and simulate the fitting curve and the *J* value of the cost function, closer to the experimental than the unfiltered data. The ARX models for the 150 and 180 rpm are:

$$\text{150 rpm: } \frac{Y(z)}{U(z)} = \frac{-0.03096 - 0.04255z^{-1} + 0.01288z^{-2}}{1 - 2.264z^{-1} + 1.551z^{-2} - 0.2863z^{-3}} \quad (4)$$

$$\text{180 rpm: } \frac{Y(z)}{U(z)} = \frac{0.1782 - 0.3172z^{-1} + 0.1416z^{-2}}{1 - 1.963z^{-1} + 0.9669z^{-2} - 0.002323z^{-3}} \quad (5)$$

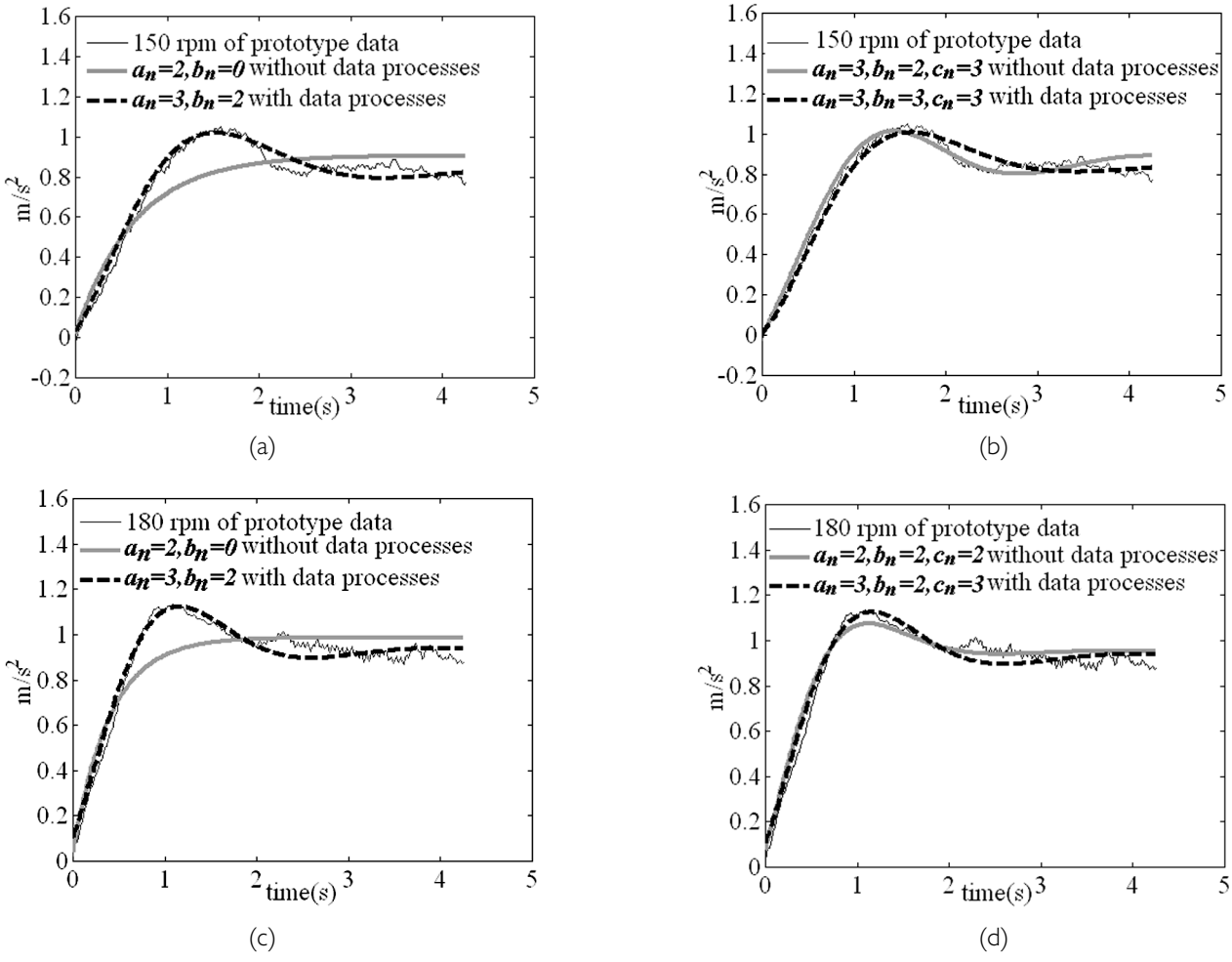

Fig 8(a): Best fitting of ARX model for 150 rpm (b): Best fitting of ARMAX model for 150 rpm (c): Best fitting of ARX model for 180 rpm (d): Best fitting of ARMAX model for 180 rpm

Converting the transfer function from the z to the s domain yields:

$$\text{150 rpm: } \frac{Y(s)}{U(s)} = \frac{0.03096s^3 + 4.028s^2 + 121.7s + 491.2}{s^3 + 75.05s^2 + 136.1s + 295.8} \quad (6)$$

$$\text{180rpm: } \frac{Y(s)}{U(s)} = \frac{0.1782s^3 + 66.89s^2 + 847.6s + 3456}{s^3 + 363.9s^2 + 842.3s + 2223}$$

The ARMAX models for the 150 and 180 rpm being:

150 rpm:

$$\frac{Y(z)}{U(z)} = \frac{0.00704 + 0.009648z^{-1} + 0.03754z^{-2} + 0.02096z^{-3}}{1 - 2.924z^{-1} + 2.85z^{-2} - 0.9266z^{-3}} \quad (7)$$

$$\text{180 rpm: } \frac{Y(z)}{U(z)} = \frac{0.1782 - 0.3167z^{-1} + 0.1411z^{-2}}{1 - 1.96z^{-1} + 0.9627z^{-2} - 0.001149z^{-3}} \quad (8)$$

Converting the transfer function from the z to the s domain gives:

$$\text{150 rpm: } \frac{Y(s)}{U(s)} = \frac{0.00704s^3 + 1.829s^2 + 10.36s + 23.57}{s^3 + 4.575s^2 + 10.18s + 13.91} \quad (9)$$

$$\text{180 rpm: } \frac{Y(s)}{U(s)} = \frac{0.1782s^3 + 74.37s^2 + 958s + 3995}{s^3 + 406.1s^2 + 986.3s + 2564} \quad (10)$$

The extremes of the ARMAX model for 150 and 180 rpm can be obtained from Equations (9) and (10), which are –2.7126, –0.9312+2.0642j, –0.9312–2.0642j, and –403.67, –1.21+2.21j, –1.21–2.21j, respectively, from which the main frequency

$$f = \frac{\omega}{2\pi}$$

of the systematic model, 0.3279Hz and 0.3517Hz and are quite similar to the main frequency shown in the experimental data. Thus, Equations (9) and (10) can serve as the transfer functions for the entire vehicle system.

Although the values of the ARX and ARMAX models for 150 and 180 rpm are different, their unit step response and performance measurements can be compared. Performance measurements include the maximum overshoot M_o, peak time t_p, rise time, and settling time.

Fig 9 shows the comparison of the best fitting of the ARX and ARMAX systematic models for 150 and 180 rpm after data process, the mathematical models having been obtained from open loop experiments. Tables 5–6 compare the performance measurements, which are not very different when

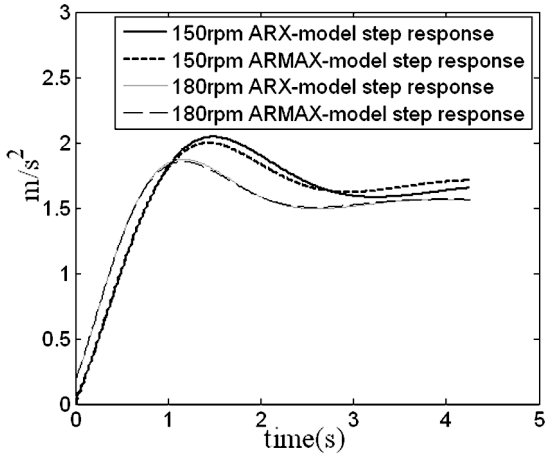

Fig 9: Comparison of the fitting results for each systematic model

	ARX-model step response	ARMAX-model step response
Maximum overshoot	23%	17%
Peak time (sec)	1.4	1.4
Rise time (sec)	0.6002371	0.6920749
Settling time (sec)	3.8795259	3.6854127

Table 5: 150 rpm ARX-model performance

comparing the ARX and ARMAX models for 150 and 180 rpm. The fitting curve of the moving average of the ARMAX model added with $e(t)$ was closer to the experimental data than that of the ARM model, also proving that the two models are suitable for system identification of the experimental vehicle.

RESULTS AND CONCLUSIONS

The current study aimed to develop a vehicle capable of navigating underwater and of capturing and transmitting data, thus enabling the system parameters of the vehicle to be identified and, hence, the system transfer functions. The vehicle adopts a modular design and independent watertight modules. The modules are connected through wired hoses and connectors to enable the transmission shaft of the actuator to function through the fixed element at the shaft centre and combine with the propeller to enable the navigation of vehicle underwater. Based on actual test and the capture and transmission of speed data in the process, the vehicle was proven to posses the capability of navigating underwater and capturing data.

The transfer functions of the entire system were obtained through system identification of the experimental vehicle. A systematic model was obtained using the ARX and ARMAX models. The filter reduced the noise to improve the accuracy of the systematic model. The J values of the cost function were obtained to compare the ARX and ARMAX models for 150 rpm and 180 rpm before and after data process.

	ARX-model step response	ARMAX-model step response
Maximum overshoot	19%	18%
Peak time (sec)	1.2	1.2
Rise time (sec)	0.5168358	0.5196622
Settling time (sec)	3.2652237	3.1815935

Table 6: 180 rpm ARMAX-model performance

Moreover, the best fitting with the experimental data was used in deciding the transfer functions of the entire system and the main frequency of the transfer function was chosen and compared with the main frequency of the experimental data for final validation.

In addition to capturing and transmitting experimental data, the dynamic performance, watertightness, and stability against conformity requirements of the experimental vehicle were tested. Problems were found during the trial navigation, included watertightness of the transmission shaft, stability adjustment, and the treatment of sensor noises.

The stability of the vehicle in water was adjusted using a counterweight. However, more counterweighing had to be implemented after the addition or removal of some devices in the vehicle. A change centre of gravity instrument can be installed in the future to solve this problem, where it can spontaneously adjust the gravity centre to avoid any shift.

Sensor signals are subject to interference mainly due to vibrations generated when the actuator operates. The sensor could be fixed into a new watertight module to reduce vibration interference and boost the accuracy and stability of the signals.

REFERENCES

1. Yandell A, Austin-Breneman J, Brett B, Brundage H, Downey J, Fantone S, Pennington T, Sheppard S, Stanway MJ and Stefanov-Wagner T. 2003. *Design of a roller-collector remotely operated vehicle.* Oceans Conference Record (IEEE) **5:** 2784–2790.

2. Gomes RMF, Sousa A, Fraga SL, Martins A, Sousa JB and Pereira FL. 2005. *A new ROV design: Issues on low drag and mechanical symmetry.* Oceans 2005 – Europe **2:** 957–962.

3. Savaresi SM, Previdi F, Dester A, Bittanti S and Ruggeri A. 2004. *Modelling, identification, and analysis of limit-cycling pitch and heave dynamics in an ROV.* IEEE Journal of Oceanic Engineering **29**(2): 407–417.

4. Koh TH, Lau MWS, Low E, Seet G, Swei S and Cheng PL. 2002. *Development and improvement of an underactuated underwater robotic vehicle.* OCEANS '2 MTS/IEEE **4:** 2039–2044.

5. Goheen KR and Jefferys ER. 1990. *The application of alternative modelling techniques to ROV dynamics.* IEEE International Conference on Robotics and Automation **2:** 1302–1309.

6. Clark L, Goheen KR and Yoerger DR. 1993. *Practical experiments in ROV system identification.* Proceedings of the 1993 American Control Conference, 575–579.

7. Touhami O, Ibtiouen R, Guechtouli A and Iung C. 2000. *Identification of SIMO system: application to an induction machine.* Industry Applications Conference **2:** 1148–1152.

8. Hsia TC. 1977. System identification: Least-squares methods. Lexington Books, Lexington, MA.

9. Ljung L. 1987. System identification: theory for the user. NJ: Prentice-Hall.

10. Ljung L. 2001. System identification toolbox for use with MATLAB, Mathworks.

11. Patcharaprakiti N, Kirtikara K, Chenvidhya D, Monyakul V and Muenpinij B. 2010. *Modelling of single phase inverter of photovoltaic system using system identification.* Computer and Network Technology 462–466.